Antarctic Science 25(6), 821–831 (2013) © Antarctic Science Ltd 2013 doi:10.1017/S0954102013000217

Salinity evolution and mechanical properties of snow-loaded multiyear sea ice near an ice shelf

A.J. GOUGH[1], A.R. MAHONEY[1,2], P.J. LANGHORNE[1] and T.G. HASKELL[3]

[1]*Department of Physics, University of Otago, PO Box 56, Dunedin 9054, New Zealand*
[2]*Geophysical Institute, University of Alaska Fairbanks, Fairbanks, AK 99775, USA*
[3]*Industrial Research Ltd, Lower Hutt, New Zealand*
ajgo@physics.otago.ac.nz

Abstract: Sea ice often forms attached to floating ice shelves. Accumulating snow can depress its freeboard, creating a flooded slush layer that may subsequently freeze to form snow ice, rejecting brine as it freezes. The resulting salinity profile determines the mechanical properties of the sea ice. We provide measurements of snow-loaded, multiyear sea ice from summer to winter. Brine from a slush layer is not completely expelled from the sea ice when the slush refreezes to form snow ice. Measurements of sea ice salinity and temperature indicate that the fate of this brine depends on the permeability of the sea ice below it. The sea ice in this study was also deformed by a nearby ice shelf over eleven years at a strain rate $\dot{\varepsilon} = (-8 \pm 3) \times 10^{-4}\,\mathrm{yr}^{-1}$ (or $3 \times 10^{-11}\,\mathrm{s}^{-1}$). From transects of sea ice thickness and structure we estimate an effective Young's modulus at medium scales for sea ice mostly composed of snow ice of $0.1\ \mathrm{GPa} < E < 0.4\ \mathrm{GPa}$, suggesting that this eleven year old sea ice cover has similar mechanical properties to warm first year sea ice. This is important for the parameterisations needed to simulate multiyear sea ice in the complex region near an ice shelf.

Received 4 July 2012, accepted 21 January 2013, first published online 19 April 2013

Key words: brine rejection, ice structure, permeability, slush layer, snow ice

Introduction

Here we investigate snow-loaded multiyear sea ice under compression by an ice shelf. Land-fast ice is common along the coast of Antarctica (Fraser *et al*. 2011), and can persist for several years (Heine 1963, Fraser *et al*. 2011). Wind flowing from the Antarctic continent deposits snow on coastal sea ice (Connolley & Cattle 1994), reducing the rate of ice growth by providing an insulating layer (e.g. Maykut & Untersteiner 1971). Snow accumulation also depresses the sea ice below sea level (Sturm *et al*. 1998). The ice surface may then flood with seawater (see Fig. 1). It is possible for this layer of slush to freeze forming 'snow ice' (e.g. Lytle & Ackley 1996, Jeffries & Adolphs 1997, Haas *et al*. 2001, Maksym & Jeffries 2001) with a texture of small interlocking crystals, a random distribution of c-axes and a higher air content than congelation ice (Gow *et al*. 1982, Lange 1988). Little information is available on the mechanical properties of multiyear sea ice where snow ice formation is an important contribution to its annual mass balance (Timco & Weeks 2010).

The fate of snow in summer affects the salinity profile of multiyear sea ice. In the Arctic snow forms melt ponds (Fetterer & Untersteiner 1998) producing a head of freshwater that flushes brine from sea ice (e.g. Eicken *et al*. 2002). The salinity of second year Arctic sea ice is typically 1 to 4, and decreases if sea ice persists for further years (e.g. Cox & Weeks 1974, Eicken *et al*. 1995). Multiyear Arctic sea ice is therefore stronger than first year ice because it has a lower brine content (Assur 1958). In the Antarctic melt ponds rarely form (Andreas & Ackley 1981, Haas *et al*. 2001) and the salinity of multiyear ice may evolve differently depending on whether there is a snow cover (e.g. Maksym & Jeffries 2000) or whether there is not (e.g. Remy *et al*. 2008).

Seawater can flood the sea ice surface in two possible ways. If the snow is warm enough to remain permeable seawater can infiltrate the snow sideways (Massom *et al*. 1998, Haas *et al*. 2001). Alternatively, if the sea ice is permeable, or is penetrated by cracks, the excess pressure at the base of the snow-laden sea ice can force seawater upwards through the ice to the surface (Hudier *et al*. 1995, Golden *et al*. 1998, Maksym & Jeffries 2000, Haas *et al*. 2001). The fate of brine when the slush refreezes is less well understood. Maksym & Jeffries (2001) simulated slush freezing above sea ice. They found that when the sea ice was impermeable brine remained in the snow ice, while if the sea ice was permeable, the brine penetrated downwards into the sea ice. Correctly modelling the movement of brine in slush layers is important when simulating biological processes in sea ice (e.g. Saenz & Arrigo 2012).

Our motivation for this study is a desire to understand the complex region in front of a calving ice tongue or ice shelf. Sea ice is the binding agent that holds icebergs within an ice mélange (e.g. Amundson *et al*. 2010), fills rifts in ice shelves (Humbert *et al*. 2009, Humbert & Steinhage 2011) and forms between icebergs after the disintegration of ice

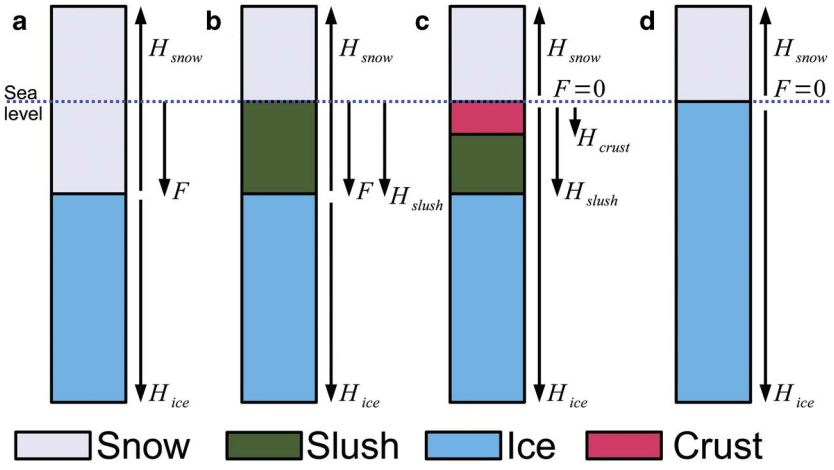

Fig. 1. Schematic of the chronology of flooding of snow on sea ice followed by freezing to form snow ice, showing the sea ice bottom ($F + H_{ice}$), snow ($F + H_{snow}$), slush (flooded snow) (H_{slush}) and crust (H_{crust}). Freeboard (F) is the height of the ice surface (top of sea ice, or crust) relative to the local sea level (blue line), and is positive if the ice surface is above the waterline. **a.** Before summer the sea ice floods only if a hole is drilled to the ocean. **b.** As the temperature rises sea ice becomes porous, or cracks allow seawater to arrive horizontally, flooding a layer of snow to form slush. **c.** In early autumn the slush layer begins to freeze forming a crust at the top of the slush layer. **d.** Finally the entire slush layer has frozen and the new snow ice becomes continuous with older ice below.

shelves (e.g. Braun *et al*. 2009). Multiyear sea ice also extends glacier tongues and ice shelves, protecting them from waves and (weakly) resisting their advance (e.g. Edgeworth David 1914, Massom *et al*. 2010, Amundson *et al*. 2010). Snow is likely to accumulate on the sea ice within the lee of large ice features so the effective mechanical properties of sea ice in these areas will therefore depend partly on the behaviour and evolution of the snow-loaded sea ice.

In this paper, which completes work initially presented by Gough *et al*. (in press), we report measurements of multiyear Antarctic fast ice where snow ice formation is combined with slow compression by the nearby ice shelf. We investigate the deformation and speculate on processes driving the evolution of the sea ice salinity profile.

Study site: multiyear sea ice in McMurdo Sound

The study was conducted at the end of summer in 2009 on multiyear sea ice near Cape Armitage, McMurdo Sound, Antarctica (Fig. 2), close to the McMurdo Ice Shelf. It is well known that in winter the sea ice of the sound is strongly influenced by conditioning of the ocean by the ice shelf, producing significant volumes of platelet ice (Leonard *et al*. 2006, Gough *et al*. 2012). Multiyear sea ice is unusual in McMurdo Sound and in 'normal' conditions fast ice breaks out in approximately one out of every two years (Heine 1963). However, because of iceberg calving from the Ross Ice Shelf, multiyear ice persisted in McMurdo Sound from 2003 (Brunt *et al*. 2006, Remy *et al*. 2008, Robinson & Williams 2012). The multiyear ice retreated each year, but by 2009 remained south of 77°40'S (Fig. 2), before fully breaking out in 2011. At our sheltered site, sea ice had been present since 1998 (Jeffrey Scanniello, personal communication 2009). When the sun was low on the horizon a pattern of rumpling was visible on the snow surface near the site, as illustrated in Fig. 3, which was also evident while driving over the sea ice. Conditions in the ocean during this experiment are described by Mahoney *et al*. (2011).

Methods

The sea ice surface and bottom (see Fig. 1), relative to sea level, was measured using a ruler, and a thickness tape through 50 mm diameter auger holes once a snow pit had been excavated to the sea ice surface. In late-February the flooded snow began to freeze, and a crust formed at the top of the flooded layer (Fig. 1c). In this case we estimated the thickness of the crust and slush layer from the feel of the drill, and report the ice surface as the top of the crust because the true ice surface was not detectable.

To investigate the buckling of the sea ice we drilled two parallel transect lines 50 m apart (x1 and x2, Fig. 2) on 5 and 13 March. We aligned these transects perpendicular to the buckling, or as close as was possible based on the surface expression. On each line ice thickness was measured at 5 m spacing as described above. When drilling both transects we encountered a slush layer but it had partially refrozen and its thickness could not be measured reliably by feel while drilling. For the second transect (x2) we first used a corer to extract the top 0.8 m of the solid ice which included the consolidating slush layer. We determined the vertical extent of the slush layer by attempting to crush the core with our bodyweight. Any part of the core which was crushed was judged to be part of the slush layer. This measurement is expected to provide only qualitative information on the extent of the slush layer.

Two pairs of hotwire gauges (Mahoney *et al*. 2009) were installed in the sea ice to monitor melt and growth at fixed locations. One pair was installed with its two gauges aligned along a peak of the rumples in the snow surface (hw-1 on Fig. 2). A second pair was installed to the side of the first transect (x1, hw-2 on Fig. 2), with gauges at positions of minimum and maximum ice thickness.

https://doi.org/10.1017/S0954102013000217 Published online by Cambridge University Press

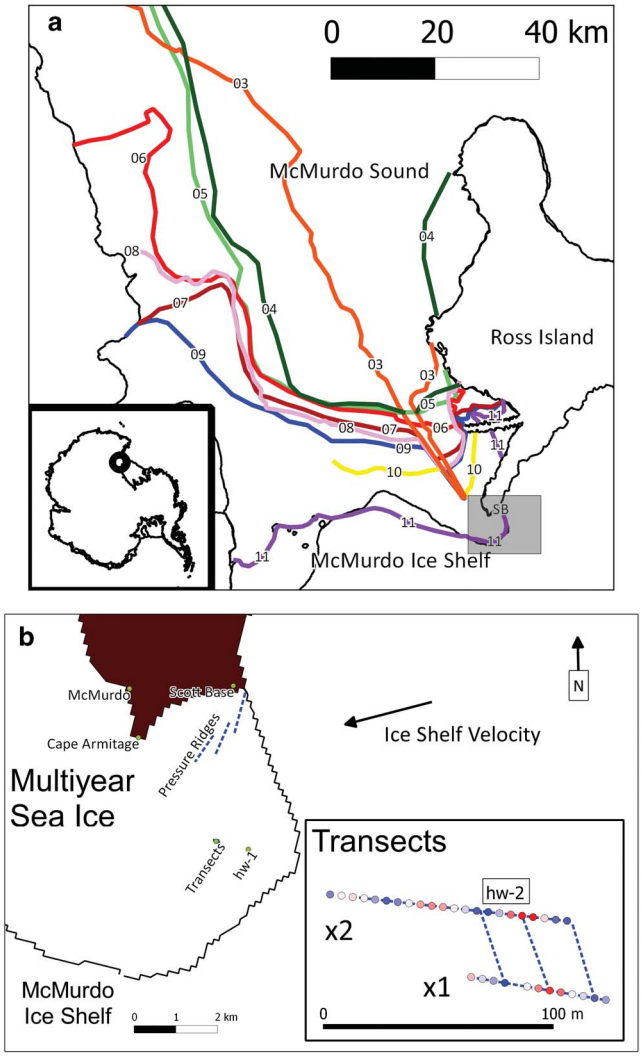

Fig. 2. We study the multiyear sea ice off Cape Armitage, the southern tip of Ross Island, in an embayment of the McMurdo Ice Shelf, Antarctica. **a.** Fast ice-edge at the end of summer from 2003–11, traced from MODIS satellite images in March of each year (2003: orange, 2004: dark green, 2005: light green, 2006: red, 2007: brown, 2008: pink, 2009: blue, 2010: yellow, 2011: purple). Initial ice shelf edge from Mosaic of Antarctica (http://lima.usgs.gov, accessed November 2011). **b.** Location of measurement sites hw-1 and hw-2 and (b. inset) main site, showing the orientation of sea ice thickness transects x1 and x2 in detail. Red shows maximum ice thickness, blue minimum ice thickness. Dashed lines connect maxima and minima. Ice shelf velocity shows direction of ice shelf advance only.

We extracted sea ice cores with 9 cm diameter. Initially cores were taken near hw-1 (Fig. 2), and, once the transects had been drilled, cores were extracted parallel to x1 and x2, offset from selected original drill holes by 5 m (see Fig. 2 for locations). Ice temperature was measured using an Omega 866C thermometer (±0.1°C).

Fig. 3. Contrast enhanced photograph of the site taken from a hill between Scott Base and McMurdo Station (Fig. 2b) shows rumpling of the snow surface highlighted while the sun was near the horizon. The Hägglunds Bv206 tracked vehicle is by hw-2 (Fig. 2b) and is 4.8 m long.

Cores were sectioned, sealed in plastic pots, and taken to Scott Base. Where a partially consolidated slush layer was present it was sampled but some brine may have drained from these samples. The bottoms of some cores were not sampled for salinity but retained for ice structure analysis. The salinity of melted samples was measured using a YSI-30 salinometer (± 0.1 in salinity). The character of the ice within all cores was noted, in particular the presence or absence of air bubbles. Cores were also taken for structural analysis, which was carried out in a cold room at -20°C. These cores were cut lengthwise and vertical thick sections were photographed illuminated through crossed polarizers. Using visual examination of the ice texture, combined with the presence or absence of large air bubbles, we classified the ice as snow-ice or congelation (either columnar or platelet) ice (e.g. Lange 1988). A number of horizontal thin sections were prepared using a microtome and crystal c-axes were measured (Langway 1958) with crystals selected on a 1 cm x 1 cm grid.

On 28 March, two weeks after the surface layer of slush had frozen completely, a short core was extracted from the top 30 cm of the hard snow ice. The snow/ice interface temperature was -7.7°C and the resulting hole did not fill with brine. This core was cooled to -20°C and transported to the cold laboratory at Scott Base. The top 12 cm of the core was split vertically, and two 1 cm thick vertical sections were cut from each facing part of the split core. These sections were then further sectioned into pieces with horizontal width 1 cm, thickness 1 cm and vertical height 3 cm (Fig. 4). Finally these samples were cleaned of cuttings and melted in individual pots. Their salinity was measured by diluting a fixed volume from the melted sample with a fixed volume of distilled water to produce a total volume large enough to be measured with the salinometer. The conductivity of these samples was measured directly, and then calibrated to salinity using a curve prepared from larger samples of sea ice measured in the same way, and measured directly. We estimate an error in these small-sample salinity measurements of ± 0.5 in salinity.

https://doi.org/10.1017/S0954102013000217 Published online by Cambridge University Press

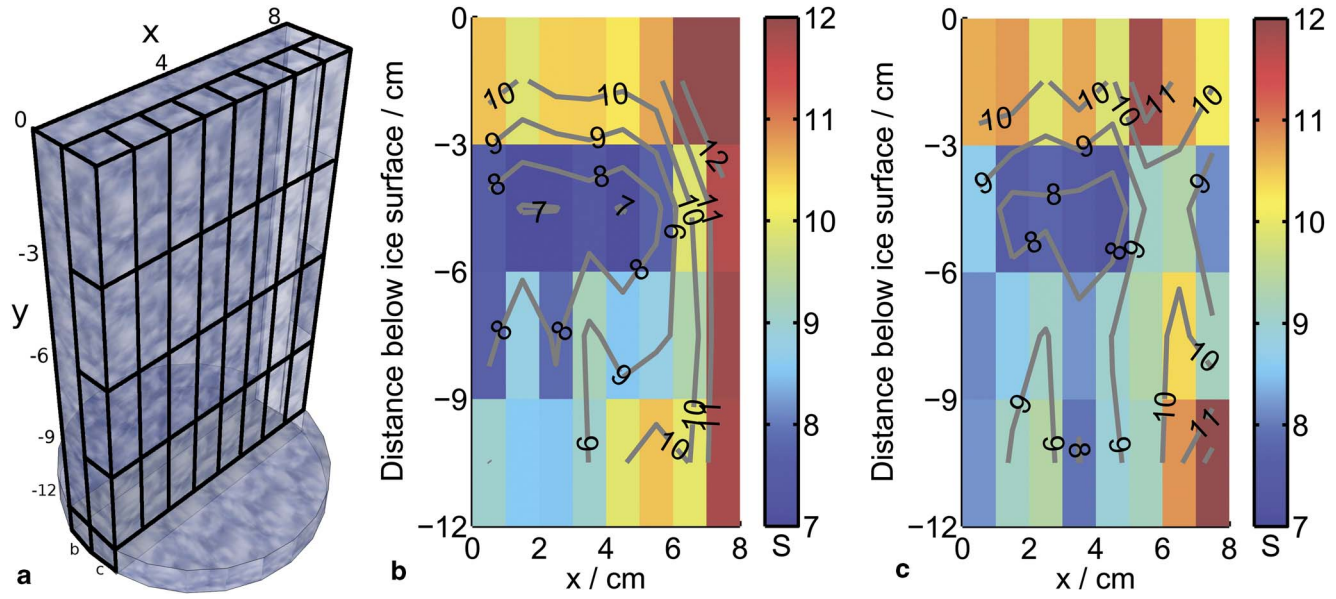

Fig. 4. a. Two vertical thick sections of snow ice cut from a core into 1 x 1 x 3 cm sections for salinity measurements at small-scale. $y = 0$ indicates the sea ice/snow interface. **b. & c.** Salinity of two 1 cm thick vertical sections in snow ice. b. & c. are from adjacent vertical sections. The top 3 cm has higher salinity than lower layers. A brine channel may exist around $x = 8$ (b. & c.).

Results

Figure 5 shows the air (T_{air}) and snow/ice interface (T_{int}) temperatures, the slush layer thickness (H_{slush}), and the position of the ice bottom (H_{ice}) at our hotwire gauges. T_{air} remained above -10°C for the first week of February then fell by 1°C per day for the next three weeks, until it reached its early-winter range, between -15°C and -25°C (Fig. 5a). T_{int} remained around -2.5°C until the first week of March, then dropped below this (Fig. 5a). In February we almost always encountered a slush layer, or a slush layer with a partially frozen crust. In mid-February the slush layer was between 0.3 m and 0.4 m thick (Fig. 5b). By mid-March, the entire ice cover again consisted of mechanically hard ice. After April the ice displayed a negative freeboard, but was not flooded at its surface (Fig. 5b). Sea ice thickness measurements from hotwires were only recorded after mid-March. However, the rate of sea ice bottom melt at both hotwire gauges was relatively constant from mid-March through to the last week of April ($dH_{ice}/dt = 2.3 \pm 0.2$ mm day^{-1}) (Fig. 5c). After mid-May, the sea ice thickened ($dH_{ice}/dt = -3.1 \pm 0.2$ mm d^{-1}) at an approximately constant rate (Fig. 5c). Although this area of sea ice was not homogeneous, we may generalize that there was a transition from sea ice with a flooded slush layer in February, to one with a dry surface and depressed freeboard by May. We did not observe any evidence of sea ice algal growth in the slush layer.

Sea ice freeboard (F), the position of the ice bottom (F - H_{ice}) and snow surface ($F + H_{snow}$) for x1 and x2 (on 5 March and 13 March) are shown in Fig. 6. For x2, the vertical extent of partially refrozen slush below a frozen crust is also shown ($F + H_{crust}$ and $F + H_{slush}$) (see Fig. 1 for F, H_{ice}, H_{snow} etc.). There is significant variation in sea ice thickness for both transects. The rumpling of H_{snow} has a smaller amplitude and is not correlated with H_{ice} (correlation between H_{ice} and H_{snow} for x1 and x2 of 0.09 and -0.21 respectively). This is not surprising as snow is shaped by wind into dunes and sastrugii, although at larger scales the surface expression of the rumpling is evident, as shown in Fig. 3. Where we were able to measure the position of the old sea ice surface (H_{slush}), the correlation between H_{ice} and H_{slush} was 0.43, indicating that both the upper and lower surfaces of the sea ice deformed in phase, so that the deformation pattern is one of buckling.

Sea ice structure at points along transects x1 and x2 is also indicated on Fig. 6. The interface between snow ice and congelation ice (H_{sc}) exaggerates the buckling pattern in H_{ice}. Thinner areas of sea ice consisted mostly of congelation ice. In contrast, thicker parts of the sea ice consisted of snow ice throughout the entire thickness, except for small amounts of congelation (columnar or platelet) ice at the base of the sea ice. Sea ice with intermediate thickness had intermediate amounts of congelation ice.

Salinity measurements from a portion of snow ice sectioned into small pieces just below the solid ice interface are shown in Fig. 4. The salinity distribution in each vertical section is similar, with elevated salinity (10–12) in the upper 3 cm of the snow ice, the lowest salinity (7–9) between 3 cm and 6 cm, and medium values of salinity (8–10) below 6 cm. A possible brine channel extends for the entire 12 cm of the vertical sections.

https://doi.org/10.1017/S0954102013000217 Published online by Cambridge University Press

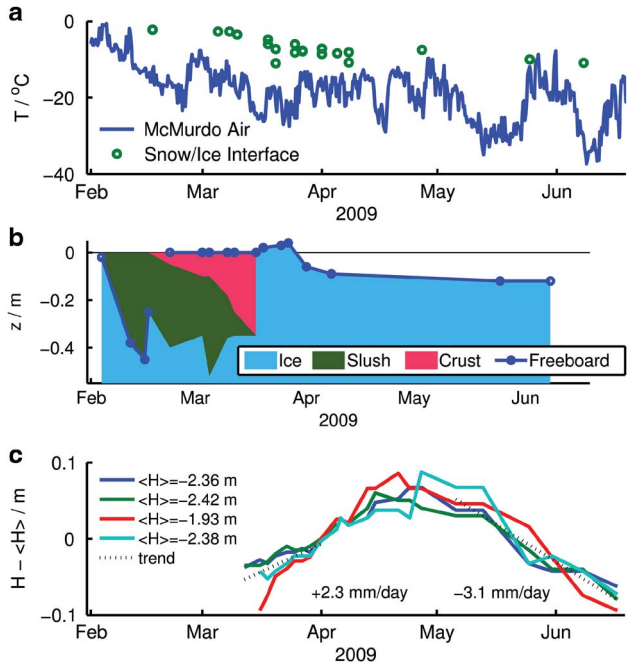

Fig. 5. a. Air and snow/ice (or snow/slush) interface temperatures. **b.** Evolution of the slush layer, initially deepening, gaining a crust and then totally freezing, after which it is not possible to distinguish this year's snow ice from previously existing snow ice. Finally the ice-freeboard decreased but the sea ice did not flood. Measurements were made at a variety of different locations. **c.** Change in the position of the ice bottom for two pairs of hotwire gauges (hw-1, hw-2 on Fig. 2b). <H> shows the mean position of the ice bottom at each gauge.

Discussion

Compression of sea ice by an advancing ice shelf

At our study site the ice displayed a pattern of buckling (Fig. 6). If this caused the ice to crack this would affect how and when seawater could flood the ice. Before discussing details, it is helpful to gain a conceptual picture of how deformation might progress over a number of years (Fig. 7). We suggest that at some time in the past a level sea ice cover formed and accumulated sufficient snow that the snow/ice interface was forced below its freeboard and a layer of snow ice formed. As time progressed, the sea ice grew and melted back each year, keeping an approximately constant thickness at the end of each summer, and forming fresh layers of snow ice each year. If there was no buckling, and if the annual snow ice formation was higher than the net annual basal melting, then layers of snow ice would be gradually transported downward, with younger snow ice above, and older snow ice below. Strong currents around Cape Armitage contribute to the high rate of basal melting in summer (e.g. Paige 1966) which is balanced over the year by surface formation of snow ice. Eventually the original snow-ice/congelation-ice interface would emerge at the base of the sea ice.

In the present circumstances, the sea ice was deformed by the nearby ice shelf, producing creep buckling (Sanderson 1988). After the first year, this would buckle the original snow-ice/congelation-ice interface. Further snow ice formation then would be expected to occur mainly in the troughs of the buckles, forming a new, level, snow/snow-ice interface. In turn, this would be deformed by buckling as would the original snow-ice/congelation-ice interface. Even after a number of years we postulate that this original snow-ice/congelation-ice interface remains preserved within the sea ice and records the total strain imposed on the sea ice since the sea ice began buckling (Fig. 7).

In Fig. 2 we show transects x1 and x2 in their wider geographical context. The direction of uniaxial compression, determined by connecting the peaks and troughs on each transect, has a bearing of 250°, which is similar to the direction of advance of the McMurdo Ice Shelf of 251° (Jeffrey Scanniello, personal communication 2009). It is therefore likely that the advancing ice shelf is the source of the stress that buckled the sea ice. An alternative source of stress is thermal expansion of confined sea ice as it warmed each spring (Johnson & Metzner 1990). In either case, the ice shelf is the root cause of the imposed stress, by either confining or directly compressing the sea ice, which is confined by the fast ice beyond Cape Armitage (Fig. 2).

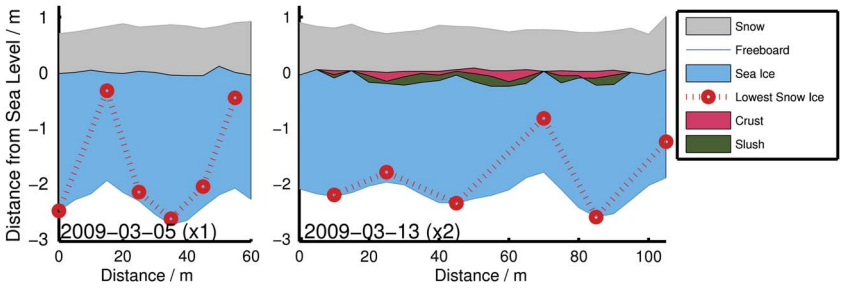

Fig. 6. Ice and snow thickness transects (see Figs 1 & 2) from March 2009. 'Snow' denotes the height of the snow cover measured at the side of each pit before drilling. 'Freeboard' is the top of the hard sea ice (F). 'Crust' and 'Slush' were only measured for x2 (see Fig. 2). 'Lowest snow ice' shows the transition in sea ice structure from snow ice (above) to congelation ice (below), determined from cores taken over the following two months.

https://doi.org/10.1017/S0954102013000217 Published online by Cambridge University Press

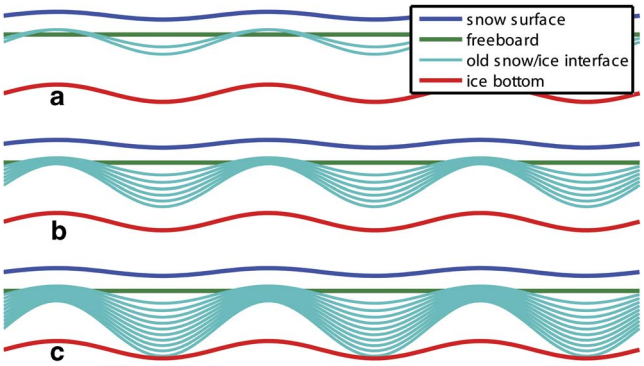

Fig. 7. Schematic of the sea ice after **a.** two, **b.** six, and **c.** ten years of snow ice formation and buckling. The snow surface and sea ice bottom are regenerated each year.

We now investigate the mechanical properties of the sea ice at a medium-scale: that is, larger than a few wavelengths of the buckling pattern. As we believe the sea ice has preserved the initial snow/congelation ice interface in the current position of the interface between snow ice and congelation ice (Figs 6 & 7) we can determine the strain imposed on the sea ice since its formation. We approximate the buckling as a sine wave so that the position of the interface can be described by:

$$H_{sc}(x) = A \sin\left(\frac{2\pi x}{\lambda}\right) + H_0, \qquad (1)$$

where A is the amplitude of the variations, λ the wavelength and H_0 the mean location of the interface. The effective strain recorded by the sea ice is:

$$\varepsilon = \lambda / L_0 - 1, \qquad (2)$$

where L_0 is the line integral of the length of the buckled surface within the sea ice (see Fig. 8):

$$L_0 = \int_0^{\lambda} \sqrt{1 + a^2 \cos^2\left(\frac{2\pi x}{\lambda}\right)}\, dx, \qquad (3)$$

where $a = 2\pi A/\lambda$, which must be numerically integrated (http://dlmf.nist.gov/17.2.ii, version 1.0.3).

From our transects (Fig. 6) we determined a wavelength for the buckling by finding the best fit of a monochromatic sine function (with any phase) to the ice bottom and the snow-ice/congelation-ice interface of each transect. The mean of these was $\lambda_t = 39.4$ m. We do not use the ice surface as that was formed from the recent freezing of a flooded slush layer, and was effectively level. The transects were not aligned with the direction of compression so we project λ_t onto this to find the true wavelength $\lambda = 35.1$ m. The amplitude of $H_{sc}(x)$ was $A = 1.08$ m. From λ and A we calculate a total effective accumulated strain $\varepsilon = -0.009 \pm 0.004$. Errors are calculated using the combinations of measured λ and A that produce the most extreme values. Assuming the ice had been present since 1998 (Jeffrey Scanniello, personal communication 2009) this translates to an effective strain rate, $\dot{\varepsilon} = (-8 \pm 3) \times 10^{-4}\ \mathrm{yr}^{-1}$ (or $3 \times 10^{-11}\ \mathrm{s}^{-1}$). Strain rates measured on the McMurdo Ice Shelf about 3 km east of our site, give strain rates of $\dot{\varepsilon} = -7.6 \times 10^{-3}\ \mathrm{yr}^{-1}$ (Stuart & Bull 1963).

Our estimate of the effective strain rate in the sea ice cover is an order of magnitude less than that for the ice shelf but the measurements of the ice shelf were made in a different location, where it is constrained by Ross Island (Fig. 2). Further, our value of A will be incorrect if parts of the original snow/sea ice interface have been melted from the bottom of the sea ice during previous summers. This is possible as we measured snow ice for the whole thickness of the sea ice at some places.

The general situation of the slow buckling of a thin floating ice sheet can be treated as that of a visco-elastic medium under axial stress supported by an elastic medium (Sjölind 1985, Sanderson 1988). We lack the necessary material parameters to analyse this situation (in particular the elastic bending stiffness of a thick sheet of snow ice, and information on the creep behaviour of warm and cold snow ice at low strain rates (Weeks 2010, Timco & Weeks 2010)). We also cannot treat the material as undergoing a constant deformation for the entire ten years of its existence, as each year it 'heals' itself by forming new snow ice on its top surface and growing layers of new sea ice at its bottom surface (which later ablate in summer). Accordingly, we will estimate the applied stress by considering only a single year of deformation, using the

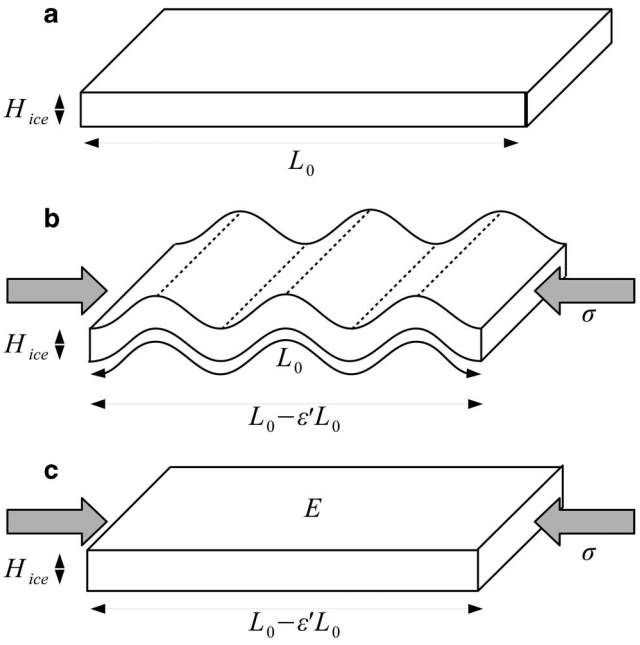

Fig. 8. Buckling of sea ice under uniaxial stress. **a.** Initially the sea ice is a flat sheet which is then **b.** buckled by an applied stress. **c.** At medium scales, we ignore the details of the buckling and treat the sea ice as a medium with an effective Young's modulus E.

https://doi.org/10.1017/S0954102013000217 Published online by Cambridge University Press

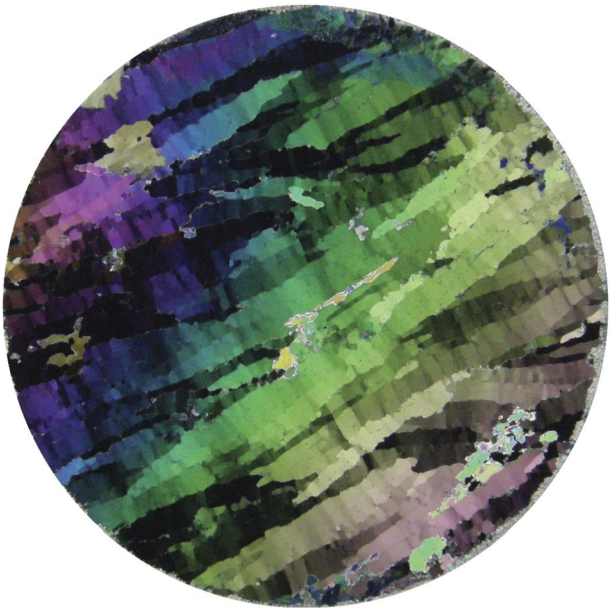

Fig. 9. Columnar ice 71 cm below the ice surface. Maximum extinction for adjacent sub-crystals within the same columnar crystal occurred at orientation differences of up to 5°.

buckling to determine the minimum work required to deform the sea ice.

After a year's deformation (see Fig. 8), neglecting energy stored as elastic bending, and energy dissipated by viscous deformation of the sea ice, the minimum energy required to buckle a floating ice sheet is the work done per unit area of sea ice by the applied stress in raising the sea ice cover against gravity or forcing it downwards against buoyancy:

$$W = Mg\Delta H - (\Delta H)^2 \rho_{sw} g/2, \tag{4}$$

where:

$$M = H_{ice}\rho_{ice} + H_{snow}\rho_{snow}, \tag{5}$$

and

$$\Delta H = A\sin(2\pi x/\lambda), \tag{6}$$

is the deviation of the ice sheet from hydrostatic equilibrium, g is the acceleration due to gravity, and ρ_{sw} is the density of seawater. As the raised and lowered parts of the sea ice cancel out over a whole wavelength the first term vanishes, giving the average energy imparted to a unit volume of the sea ice (assuming the snow does not contribute to the mechanical properties of the cover):

$$\overline{W} = \frac{A^2 \rho_{sw} g}{4H_{ice}}. \tag{7}$$

This work is done by the applied stress on a unit area of sea ice. Taking the one year's effective strain, ε_1, we determine the amplitude of buckling after one year, $A_1 = 0.34$ m (by iteratively solving Eqs (1) & (2)). This yields a stored energy per unit volume of the sea ice, $\overline{W} = 116\,\mathrm{J\,m^{-3}}$

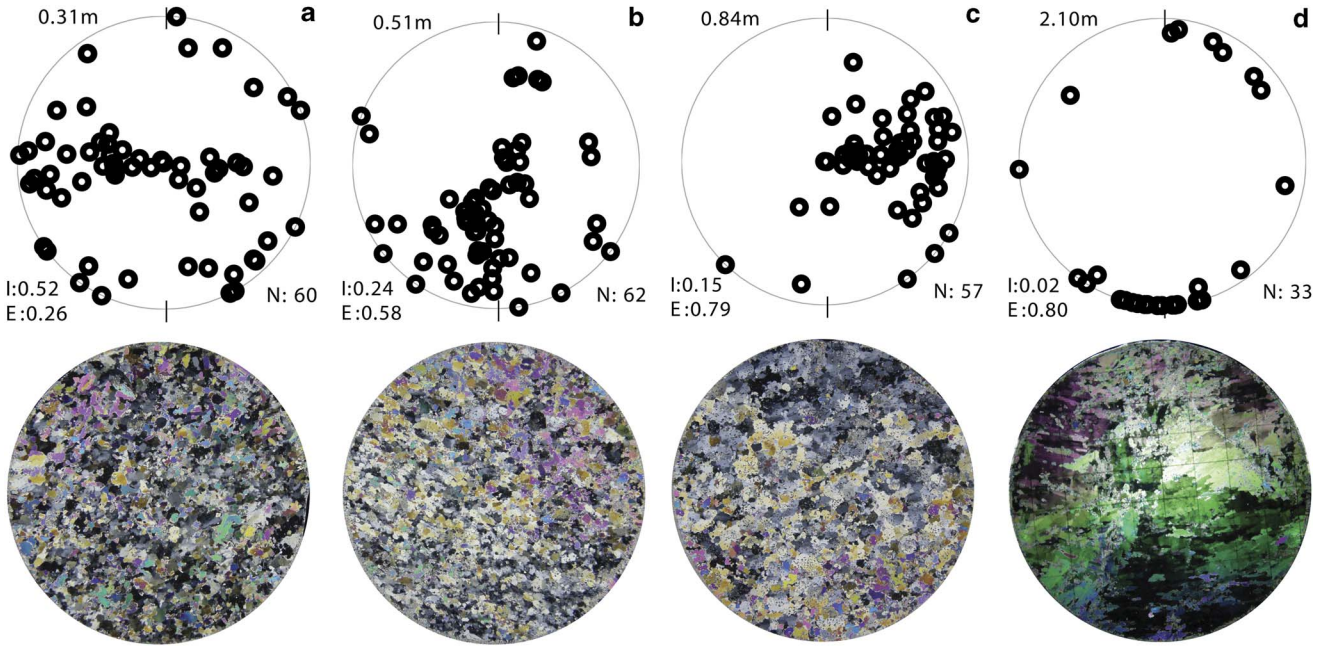

Fig. 10. C-axis measurements and thin sections. **a., b. & c.** Snow ice from one core on transect x1. **d.** Columnar ice from a core at hw-1. z indicates distance below ice surface. N shows the number of c-axes measurements taken. Thin sections are 9 cm in diameter. All subfigures are oriented with up (on the page) parallel with the line of transects x1 and x2.

https://doi.org/10.1017/S0954102013000217 Published online by Cambridge University Press

for $H_{ice} = 2.5$ m. Let us now ignore the details of the buckling (see Fig. 8) and assume that this energy per unit volume is imparted by a constant uniaxial compressive stress action (σ) over one year. This implies that:

$$\sigma = \frac{\overline{W}}{\varepsilon_1}, \tag{8}$$

so that $\sigma = 140$ kPa. Sea ice can fail by being crushed. For 2 m thick first year sea ice the uniaxial crushing strength is in the range 2–4 MPa (Sanderson 1988), with 2 MPa being appropriate for high porosity sea ice in summer. Pressure ridges are present in the area we studied, but only at locations away from our measurement site where the stress in the sea ice might be enhanced as it was forced against the coastline (Fig. 2). Accordingly, we regard 2 MPa as an upper limit for σ.

From our value of σ we estimate an effective Young's modulus for floes composed mostly of snow ice of $E = \sigma/\varepsilon_1 = 0.18$ GPa for deformation at medium scales. The sea ice thickness varied from 2–3 m, and our estimate of ε_1 has an error of 3×10^{-4}, so E ranges from 0.1–0.4 GPa. We have calculated a minimum stress as we neglect elastic and viscous processes, and we used a conservative estimate for A, so we expect that we have obtained a lower bound for E.

It is possible that this multiyear ice relieved some of the imposed stress through creep. It is difficult to uniquely determine the stress-strain history of a sample purely from inspection of its crystal fabric (Rigsby 1968, Gow & Williamson 1976). Nonetheless, departure of the fabric from its initial state indicates that mechanical deformation has occurred (Cuffey & Paterson 2010, Treverrow *et al.* 2012). In undeformed congelation ice we expect an entire crystal to have the same alignment. In the columnar sea ice we sampled (Fig. 9) subgrains show variations in alignment of 5°, called striations. Similar striations were reported in a sea ice sample from the pressure ridges near Scott Base (Fig. 2) by Paige (1966). In snow ice, where we expect a uniform distribution of c-axis orientations (Lange 1988), the youngest (highest) snow ice fabric was moderately uniform, but lower in the sea ice the fabric became less uniform (Fig. 10). We have only a limited number of c-axes measurements, so strong conclusions cannot be drawn, nevertheless, our measurements suggest that it is likely that some of the stress imposed on the sea ice was accommodated through irreversible creep at small scales.

Where $\varepsilon > 0.01$, polycrystalline pure ice enters tertiary creep associated with the formation of microcracks at boundaries between ice crystals. These microcracks can coalesce and lead to failure of the material (Sanderson 1988, Cuffey & Paterson 2010), especially at the top of the ridges and the bottom of the troughs of the buckling, as those will be areas where the sea ice is locally under tension (Sanderson 1988). This cracking could penetrate the ice cover and might provide a route for seawater to flood the sea ice. For our experiment it is possible that over ten years the effective strain is greater than 0.01. Nevertheless, the sea ice can 'heal' damage due to temperature cycling in the sea ice from winter, through summer, and back to winter. Such changes cause 5–10% of the ice to melt (because the brine volume fraction φ_l varies with T), and refreeze. The parts of the sea ice most likely to crack (at the snow/sea ice interface and at the base) are either renewed each year as new snow ice forms, or fresh ice grows at the base each winter and is melted away in summer (Fig. 5). Accordingly the real strain may locally be less than ε measured at medium scales. We conclude that it is unlikely that cracks persisted from year to year so seawater most likely flooded to the surface by percolating upwards in the sea ice brine channel network once it became permeable in the summer.

For comparison with our estimate of E, at very low stress rates, Tabata *et al.* (1967) reported E for warm first year sea ice samples in the range 0.2–0.4 GPa, while Mahoney *et al.* (2004) estimated $E = 0.07$ GPa for nearly isothermal first year sea ice. These samples, from sea ice with high salinity and brine fraction, are similar to our estimate of E for warm multiyear sea ice. It is therefore important to examine the brine content of this sea ice and the factors that control it.

Brine transport in multiyear snow ice

We now investigate the fate of brine as snow-loaded multiyear sea ice floods and subsequently freezes. We begin by considering centimetre-scale variations in the salinity of recently formed snow ice (Fig. 4). We measured enhanced salinity in the uppermost 3 cm of the snow ice. This higher salinity in the very top layer might be a reflection of the effect seen by Worster & Wettlaufer (1997), where brine did not initially drain from a thin ice sheet growing into a salt solution. We might expect the same process to occur even when brine freezes within a pre-existing matrix of snow crystals. Alternatively, this observation may simply be the result of variations in snow density. The amount of brine present initially in the slush fills the spaces in the snow. We would expect the snow to be relatively homogeneous horizontally, but to show significant vertical variability.

The potential presence of a brine channel ($x = 8$ on Fig. 4) is also interesting as these were not visible in photographs of the thick sections (not shown). This vertical region of enhanced salinity could be the result of brine draining to one side of the sample during transport or storage, but we extracted the core once the snow ice had refrozen and air and ice temperatures were low enough that the sea ice was unlikely to be permeable when we sampled it (Fig. 5a). The presence of a brine channel supports the simulations of Maksym & Jeffries (2001) which produced convective features and vertical regions of enhanced salinity.

https://doi.org/10.1017/S0954102013000217 Published online by Cambridge University Press

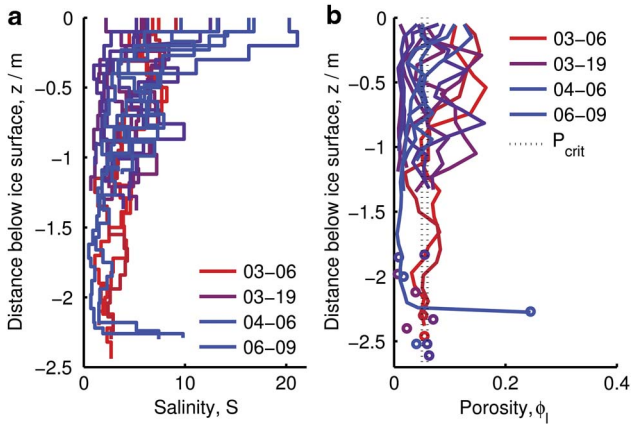

Fig. 11. a. Sea ice salinity, and **b.** porosity from cores, coloured by date extracted (month-day). Where cores did not cover the entire ice thickness, a small circle has been plotted at the 'base' of the ice. P_{crit} shows a porosity of 0.05–0.06, where we expect a transition between permeable and impermeable sea ice. Some cores lack temperature profiles so only salinity is shown.

Our centimetre-scale salinity measurements also reproduce some of the features seen when granular ice is formed from a prepared slush in a laboratory. Tison & Verbeke (2001) reported enhanced salinity in the highest layer of the ice, and significant horizontal variation. They report higher salinity than we see in our snow ice, which may be due to faster growth rates in their experiment or a higher initial ice fraction due to compacted snow in ours.

We now consider the porosity of the full thickness of the sea ice. We can combine our measurements of sea ice temperature and salinity to determine the brine volume fraction, φ_l (Cox & Weeks 1983). We are unable to account for the air content of the ice. Salinity and φ_l are shown in Fig. 11. In early March, in the upper 0.5 m of the sea ice, we see that φ_l has a value above the porosity of 0.05 at which permeability drops rapidly towards zero (Golden *et al*. 1998, Maksym & Jeffries 2000). In the lower 1 m of the sea ice φ_l is close to this critical value. As the sea ice cooled, porosity decreased first at the surface, then deeper in the sea ice. By May, the sea ice-freeboard was noticeably negative (Fig. 5b), but it did not flood until pierced by drilling, indicating that the sea ice cover was no longer permeable.

The sea ice surface was flooded in February, so we view the salinity profile as being a result of the flooding process. The sea ice was under compression so it is unlikely that cracks existed locally which penetrated the full thickness of the sea ice to allow seawater to arrive horizontally. Further, the buckling in the sea ice raised occasional barriers to horizontal infiltration (Fig. 6). Instead it seems that seawater percolated upwards sometime in the summer once the sea ice had warmed enough to become just-permeable. At this time seawater must enter the sea ice matrix and displace brine to flood the sea ice surface and fill the voids in the snow above. If we take a reasonable initial snow porosity of 0.5, and $F = -0.2$ m this implies that 0.1 m of fluid had to reach the sea ice surface. At a temperature of -2.5°C (so brine salinity, $S_{brine} = 45$) and a bulk salinity of 2.5 the sea ice initially contained only 0.1 m of brine (Cox & Weeks 1983) per unit area. Thus seawater with $S_{sw} = 35$ replaces brine in the sea ice with $S_{brine} = 45$. As the sea ice is still colder than the freezing point of seawater, some of the seawater will freeze, slightly warming the sea ice, but also reducing the porosity of the sea ice by replacing liquid with ice. Throughout the summer this feedback will cause the sea ice to remain close to the threshold between being permeable and impermeable. Any slight warming will allow more seawater to penetrate, which in turn will freeze, returning the sea ice to a state of critical permeability, so long as it remains colder than the freezing point of seawater. Rapid bottom melting (Fig. 5c) maintains increased pressure at the base of the sea ice, encouraging upward motion of brine.

While somewhat speculative, as we were not able to follow its evolution, this process would produce sea ice with the characteristics we measured when we arrived in February, with a flooded snow layer with high salinity, a layer of sea ice with enhanced salinity and, below that, sea ice with a salinity and temperature which cause it to be close to the critical permeability. However, a purely upward transport of brine is not likely, as we will see by considering the fate of the salt within the sea ice as it freezes.

The mean salinity of the top 0.1 m of sea ice after consolidation (11 cores taken after 15 March) was 9.5 (Fig. 11). With a snow fraction of 0.5 and no loss of brine we would expect S = 17.5 if a 1:1 snow-seawater mix had frozen. Some brine was therefore able to leave the layer of slush. We see little change in the salinity of the lowest sea ice below 1.5 m depth, even after the slush had consolidated, but we do perhaps see an increase in salinity in the top 0.5 m of the sea ice. Brine rejected from the slush layer penetrates the top 0.5 m of the sea ice. Below this the sea ice cooled too rapidly for the brine to sink all the way through the sea ice to the ocean. Although not shown here, very little brine was expelled into the snow cover.

This means that the salt is trapped in the upper 1 m of the sea ice over the winter. If the sea ice has a negative freeboard by summer and becomes permeable and only upward transport of brine occurred, we would see salt concentrating in the slush layer, and in the upper layer of the sea ice formed once the slush had refrozen. As the sea ice at our study site has passed through a number of annual cycles, and does not show significantly enhanced salinity in its upper layers, there must be a period during the summer (when we were not present) during which the sea ice lost the brine which had accumulated in previous seasons to produce the initial bulk salinity of around 2.5 that we observed. This suggests that there is either an exchange of

https://doi.org/10.1017/S0954102013000217 Published online by Cambridge University Press

brine with seawater over the summer, or that the flooding process of the sea ice is partially or entirely through horizontal infiltration of seawater at the surface, which we do not believe was likely.

Our salinity, temperature and porosity measurements of the full thickness of the multiyear sea ice, and our small-sample salinity measurements from the upper 12 cm of recently formed snow ice, support the simulations of Maksym & Jeffries (2001). The slush layer loses brine to the sea ice below as it freezes, which we observed in the lower than expected salinity of recently frozen slush layers, and slightly elevated salinity in the sea ice down to 0.5 m. This demonstrates that the permeability of the underlying sea ice is important when considering the desalination of slush layers. In our study brine was trapped in the upper part of the sea ice and presumably did not undergo constant exchange with the ocean which has been reported by other studies (e.g. Lytle & Ackley 1996, Saenz & Arrigo 2012). This limits the supply of nutrients to the slush layer and perhaps explains the lack of observed algal layers in the slush at our site.

Finally we note that the brine fractions at our snow-laden multiyear sea ice site are closer to those of first year sea ice than to typical multiyear sea ice of the Arctic (Weeks 2010). Since brine fraction is a pivotal parameter in determining the mechanical behaviour (Timco & Weeks 2010), we suggest that the properties of first year sea ice are naturally appropriate here.

Conclusions

We studied an area of snow-loaded multiyear Antarctic fast ice over five months as the sea ice evolved from summer melt to winter freeze-up. This multiyear sea ice was composed mostly of snow ice and had a thickness at the end of summer 2009 between 1.8 and 2.5 m and a snow cover of between 0.8 and 1.0 m. Snow loading depressed the freeboard, leading to flooding by seawater and the formation of a slush layer. This slush layer subsequently froze to form snow ice. While it was not part of an ice mélange, its evolution offers useful insights into the physical and mechanical behaviour of the sea ice that binds icebergs together and fills rifts in some ice shelves.

By studying the evolution of the sea ice salinity profile we demonstrated that brine from the slush layer that forms at the sea ice surface in summer is not able to completely leave the sea ice when that layer refreezes to form snow ice in winter. Nevertheless, the salinity profile that evolved over a number of years suggests that brine leaves the sea ice at some stage of the year, presumably in the warmest part of summer between December and February. The flooding mechanism, whether through horizontal infiltration, upward flushing with seawater, or a mixture of both, results in more saline multiyear sea ice than is typical of the Arctic. The temperature and salinity of the ice early in February (T ~ -2.5°C, salinity ~ 2.5) suggest that it was maintained on the limit of being permeable. This behaviour will have implications for the transport of nutrients within sea ice in these areas.

The sea ice displayed significant buckling, probably caused by the advance of the McMurdo Ice Shelf. By drilling thickness transects and from ice structure measurements we determined a wavelength for the buckling of $\lambda = 35$ m. The interface between snow ice and congelation ice exaggerated the buckling pattern of the ice/ocean or ice/snow interfaces, leading us to speculate that this preserved the original sea ice/snow interface, and allowing us to calculate an effective strain rate $\dot{\varepsilon} = (-8 \pm 3) \times 10^{-4}\,\mathrm{yr}^{-1}$ (or $3 \times 10^{-11}\,\mathrm{s}^{-1}$). We observed further evidence of creep in striated thin sections and non-isotropic c-axis fabrics. Finally we estimated an effective Young's modulus for multiyear sea ice composed of snow ice in the range $0.1\,\mathrm{GPa} < E < 0.4\,\mathrm{GPa}$ which is similar to those measured for warm first year sea ice (Timco & Weeks 2010). Given that the salinity of the multiyear snow ice is similar to first year sea ice this result is, in hindsight, not surprising. Our estimate of E may be useful to those seeking to model an ice mélange.

Acknowledgements

We thank Brian Staite, Euan Paterson and the 2009 Scott Base winter team for assistance in the field. This work, part of New Zealand's contribution to the IPY, was funded by the Foundation for Research, Science and Technology and a University of Otago postgraduate scholarship. The Rt Hon William R. Chandler also donated generously to the project. Logistical support was provided by Antarctica New Zealand. We thank Mike Williams and Jean-Louis Tison for their comments and Jeff Scanniello for information on the breakout history at Cape Armitage prior to 2003. We also gratefully acknowledge the constructive comments of the reviewer.

References

Amundson, J.M., Fahnestock, M., Truffer, M., Brown, J., Lthi, M.P. & Motyka, R.J. 2010. Ice mélange dynamics and implications for terminus stability, Jakobshavn Isbrae, Greenland. *Journal of Geophysical Research*, 10.1029/2009JF001405.

Andreas, E.L. & Ackley, S.F. 1981. On the differences in ablation seasons of Arctic and Antarctic sea ice. *Journal of Atmospheric Science*, **39**, 440–447.

Assur, A. 1958. Composition of sea ice and its tensile strength. *In Arctic sea ice. Proceedings of the conference held at Easton, Maryland, 24–27 February 1958.* Washington, DC: US National Academy of Sciences, National Research Council, Publication No. 598, 106–138.

Braun, M., Humbert, A. & Moll, A. 2009. Changes of Wilkins Ice Shelf over the past 15 years and inferences on its stability. *The Cryosphere*, **3**, 41–56.

Brunt, K., Sergienko, O. & MacAyeal, D. 2006. Observations of unusual fast-ice conditions in the southwest Ross Sea, Antarctica: preliminary analysis of iceberg and storminess effects. *Annals of Glaciology*, **44**, 183–187.

Connolley, W.M. & Cattle, H. 1994. The Antarctic climate of the UKMO Unified Model. *Antarctic Science*, **6**, 115–122.

Cox, G.F.N. & Weeks, W.F. 1974. Salinity variations in sea ice. *Journal of Glaciology*, **13**, 109–120.

Cox, G.F.N. & Weeks, W.F. 1983. Equations for determining the gas and brine volumes in sea ice samples. *Journal of Glaciology*, **29**, 306–316.

Cuffey, K. & Paterson, W.S.B. 2010. *The physics of glaciers*, 4th ed. Burlington, MA: Butterwort-Heinemann, 704 pp.

Edgeworth David, T.W. 1914. Antarctica and some of its problems. *The Geographical Journal*, **43**, 605–627.

Eicken, H., Krouse, H.R., Kadko, D. & Perovich, D.K. 2002. Tracer studies of pathways and rates of meltwater transport through Arctic summer sea ice. *Journal of Geophysical Research*, 10.1029/2000JC000583.

Eicken, H., Lensu, M., Leppranta, M., Tucker, W.B.I., Gow, A.J. & Salmela, O. 1995. Thickness, structure, and properties of level summer multiyear ice in the Eurasian sector of the Arctic Ocean. *Journal of Geophysical Research*, **100**, 22 697–22 710.

Fetterer, F. & Untersteiner, N. 1998. Observations of melt ponds on Arctic sea ice. *Journal of Geophysical Research*, **103**, 24 821–24 835.

Fraser, A.D., Massom, R.A., Michael, K.J., Galton-Fenzi, B.K. & Lieser, J.L. 2011. East Antarctic landfast sea ice distribution and variability, 2000–2008. *Journal of Climate*, **25**, 1137–1156.

Golden, K.M., Ackley, S.F. & Lytle, V.I. 1998. The percolation phase transition in sea ice. *Science*, **282**, 2238–2241.

Gough, A.J., Mahoney, A.R., Langhorne, P.J., Williams, M.J.M. & Haskell, T.G. In press. *Multiyear sea ice near an ice shelf: mechanical properties and brine migration in snow ice. In Proceedings of the 21st IAHR International Symposium on Ice, Dalian, China, 11–15 June 2012*. Dalian: Dalian University of Technology Press.

Gough, A.J., Mahoney, A.R., Langhorne, P.J., Williams, M.J.M., Robinson, N.J. & Haskell, T.G. 2012. Signatures of supercooling: McMurdo Sound platelet ice. *Journal of Glaciology*, **58**, 38–50.

Gow, A.J. & Williamson, T. 1976. Rheological implications of the internal structure and crystal fabrics of the West Antarctic ice sheet as revealed by deep core drilling at Byrd Station. *Geological Society of America Bulletin*, **87**, 1665–1677.

Gow, A.J., Ackley, S., Weeks, W. & Govoni, J. 1982. Physical and structural characteristics of Antarctic sea ice. *Annals of Glaciology*, **3**, 113–117.

Haas, C., Thomas, D. & Bareiss, J. 2001. Surface properties and processes of perennial Antarctic sea ice in summer. *Journal of Glaciology*, **47**, 613–625.

Heine, A. 1963. Ice breakout around the southern end of Ross Island, Antarctica. *New Zealand Journal of Geology and Geophysics*, **6**, 395–401.

Hudier, E.-J., Ingram, R. & Shirasawa, K. 1995. Upward flushing of seawater through first year ice. *Atmosphere-Ocean*, **33**, 569–580.

Humbert, A. & Steinhage, D. 2011. The evolution of the western rift area of the Fimbul Ice Shelf, Antarctica. *The Cryosphere*, **5**, 931–944.

Humbert, A., Kleiner, T., Mohrholz, C.-O., Oelke, C., Greve, R. & Lange, M.A. 2009. A comparative modeling study of the Brunt Ice Shelf/Stancomb-Wills Ice Tongue system, East Antarctica. *Journal of Glaciology*, **55**, 53–65.

Jeffries, M.O. & Adolphs, U. 1997. Early winter ice and snow thickness distribution, ice structure and development of the western Ross Sea pack ice between the ice-edge and the Ross Ice Shelf. *Antarctic Science*, **9**, 188–200.

Johnson, J.B. & Metzner, R.C. 1990. Thermal expansion coefficients for sea ice. *Journal of Glaciology*, **36**, 343–349.

Lange, M.A. 1988. Basic properties of Antarctic sea ice as revealed by textural analysis of ice cores. *Annals of Glaciology*, **10**, 95–101.

Langway, C.C. 1958. Ice fabrics and the universal stage. *CRREL Technical Report*, No. 62, 16 pp.

Leonard, G.H., Purdie, C.R., Langhorne, P.J., Haskell, T.G., Williams, M.J.M. & Frew, R.D. 2006. Observations of platelet ice growth and oceanographic conditions during the winter of 2003 in McMurdo Sound, Antarctica. *Journal of Geophysical Research*, 10.1029/2005JC002952.

Lytle, V.I. & Ackley, S.F. 1996. Heat flux through sea ice in the western Weddell Sea: convective and conductive transfer processes. *Journal of Geophysical Research*, **101**, 8853–8868.

Mahoney, A., Eicken, H., Shapiro, L. & Grenfell, T.C. 2004. Ice motion and driving forces during a spring ice shove on the Alaskan Chukchi coast. *Journal of Glaciology*, **50**, 195–207.

Mahoney, A., Gearheard, S., Oshima, T. & Qillaq, T. 2009. Sea ice thickness measurements from a community based observing network. *Bulletin of the American Meteorological Society*, **90**, 370–377.

Mahoney, A.R., Gough, A.J., Langhorne, P.J., Robinson, N.J., Stevens, C.L., Williams, M.M.J. & Haskell, T.G. 2011. The seasonal appearance of ice shelf water in coastal Antarctica and its effect on sea ice growth. *Journal of Geophysical Research*, 10.1029/2011JC007060.

Maksym, T. & Jeffries, M.O. 2000. A one-dimensional percolation model of flooding and snow ice formation on Antarctic sea ice. *Journal of Geophysical Research*, **105**, 26 313–26 331.

Maksym, T. & Jeffries, M.O. 2001. Phase and compositional evolution of the flooded layer during snow-ice formation on Antarctic sea ice. *Annals of Glaciology*, **33**, 37–44.

Massom, R.A., Lytle, V.I., Worby, A.P. & Allison, I. 1998. Winter snow cover variability on East Antarctic sea ice. *Journal of Geophysical Research*, **103**, 24 837–24 855.

Massom, R.A., Giles, A.B., Fricker, H.A., Warner, R.C., Legrésy, B., Hyland, G., Young, N. & Fraser, A.D. 2010. Examining the interaction between multi-year landfast sea ice and the Mertz Glacier Tongue, East Antarctica: another factor in ice sheet stability? *Journal of Geophysical Research*, **115**, 10–55.

Maykut, G.A. & Untersteiner, N. 1971. Some results from a time-dependent thermodynamic model of sea ice. *Journal of Geophysical Research*, **76**, 2–4.

Paige, R.A. 1966. Crystallographic studies of sea ice in McMurdo Sound, Antarctica. *U.S. Naval Civil Engineering Laboratory, Technical Report* R494, 31 pp.

Remy, J.-P., Becquevort, S., Haskell, T.G. & Tison, J.-L. 2008. Impact of the B-15 iceberg "stranding event" on the physical and biological properties of sea ice in McMurdo Sound, Ross Sea, Antarctica. *Antarctic Science*, **20**, 593–604.

Rigsby, G. 1968. The complexities of the three-dimensional shape of individual crystals in glacier ice. *Journal of Glaciology*, **7**, 233–251.

Robinson, N.J. & Williams, M.J.M. 2012. Iceberg-induced changes to polynya operation and regional oceanography in the southern Ross Sea, Antarctica, from *in situ* observations. *Antarctic Science*, **24**, 514–526.

Saenz, B.T. & Arrigo, K.R. 2012. Simulation of a sea ice ecosystem using a hybrid model for slush layer desalination. *Journal of Geophysical Research*, 10.1029/2011JC007544.

Sanderson, T.J.O. 1988. *Ice mechanics: risks to offshore structures*. London: Graham & Trotman, 253 pp.

Sjölind, S.-G. 1985. Visco-elastic buckling analysis of floating ice sheets. *Cold Regions Science and Technology*, **11**, 241–246.

Stuart, A.W. & Bull, C. 1963. Glaciological observations on the Ross Ice Shelf near Scott Base, Antarctica. *Journal of Glaciology*, **4**, 399–414.

Sturm, M., Morris, K. & Massom, R. 1998. The winter snow cover of the west Antarctic pack ice: its spatial and temporal variability. *Antarctic Research Series*, **74**, 1–18.

Tabata, T., Fujino, K. & Aota, M. 1967. Studies of the mechanical properties of sea ice: the flexural strength of sea ice *in situ*. *In* Ôura, H., *ed. Physics of snow and ice*. Sapporo: Institute of Low Temperature Science, Hokkaido University, 539–550.

Timco, G. & Weeks, W. 2010. A review of the engineering properties of sea ice. *Cold Regions Science and Technology*, **60**, 107–129.

Tison, J.-L. & Verbeke, V. 2001. Chlorinity/salinity distribution patterns in experimental granular sea ice. *Annals of Glaciology*, **33**, 13–20.

Treverrow, A., Budd, W.F., Jacka, T.H. & Warner, R.C. 2012. The tertiary creep of polycrystalline ice: experimental evidence for stress-dependent levels of strain-rate enhancement. *Journal of Glaciology*, **58**, 301–314.

Weeks, W.F. 2010. *On sea ice*. Fairbanks, AK: University of Alaska Press, 664 pp.

Worster, M.G. & Wettlaufer, J.S. 1997. Natural convection, solute trapping, and channel formation during solidification of saltwater. *Journal of Physical Chemistry*, **B101**, 6132–6136.